Redox Biology 32 (2020) 101493

Contents lists available at ScienceDirect

Redox Biology

journal homepage: www.elsevier.com/locate/redox

Induction of caveolin-3/eNOS complex by nitroxyl (HNO) ameliorates diabetic cardiomyopathy

Hai-Jian Sun[a], Si-Ping Xiong[a], Zhi-Yuan Wu[a], Lei Cao[a], Meng-Yuan Zhu[a], Philip K. Moore[a], Jin-Song Bian[a,b,*]

[a] Department of Pharmacology, Yong Loo Lin School of Medicine, National University of Singapore, Singapore, 117597, Singapore
[b] National University of Singapore (Suzhou) Research Institute, Suzhou, China

ARTICLE INFO

Keywords:
Nitroxyl
Cardiomyocytes
Diabetes
Oxidative stress
Apoptosis

ABSTRACT

Nitroxyl (HNO), one-electron reduced and protonated sibling of nitric oxide (NO), is a potential regulator of cardiovascular functions. It produces positive inotropic, lusitropic, myocardial anti-hypertrophic and vasodilator properties. Despite of these favorable actions, the significance and the possible mechanisms of HNO in diabetic hearts have yet to be fully elucidated. H9c2 cells or primary neonatal mouse cardiomyocytes were incubated with normal glucose (NG) or high glucose (HG). Male C57BL/6 mice received intraperitoneal injection of streptozotocin (STZ) to induce diabetes. Here, we demonstrated that the baseline fluorescence signals of HNO in H9c2 cells were reinforced by both HNO donor Angeli's salt (AS), and the mixture of hydrogen sulfide (H_2S) donor sodium hydrogen sulfide (NaHS) and NO donor sodium nitroprusside (SNP), but decreased by HG. Pretreatment with AS significantly reduced HG-induced cell vitality injury, apoptosis, reactive oxygen species (ROS) generation, and hypertrophy in H9c2 cells. This effect was mediated by induction of caveolin-3 (Cav-3)/endothelial nitric oxide (NO) synthase (eNOS) complex. Disruption of Cav-3/eNOS by pharmacological manipulation or small interfering RNA (siRNA) abolished the protective effects of AS in HG-incubated H9c2 cells. In STZ-induced diabetic mice, administration of AS ameliorated the development of diabetic cardiomyopathy, as evidenced by improved cardiac function and reduced cardiac hypertrophy, apoptosis, oxidative stress and myocardial fibrosis without affecting hyperglycemia. This study shed light on how interaction of NO and H_2S regulates cardiac pathology and provide new route to treat diabetic cardiomyopathy with HNO.

1. Introduction

Diabetes is closely related to both microvascular and macrovascular complicates. The later is responsible for high incidence of cardiovascular diseases including stroke, myocardial infarction and peripheral vascular diseases [1]. As a common complication of diabetes, diabetic cardiomyopathy (DCM) is believed to be responsible for the morbidity and mortality among diabetic patients [2]. DCM is manifested by various structural and functional anomalies in the myocardium, such as cardiomyocyte hypertrophy, myocardial fibrosis, cardiac autonomic neuropathy and apoptosis, as well as left ventricular diastolic and systolic dysfunction [3]. These characteristics of DCM are prognostic indicators for mortality in diabetic patients [3]. Hence, development of novel therapeutic strategies or discovery of new pharmacological targets to treat DCM is paramount.

Accumulating evidence has revealed that systemic and sterile inflammation, excessive reactive oxygen species (ROS) generation, insufficiency of antioxidant systems, impaired endothelial nitric oxide (NO) synthase (eNOS)/NO signaling, mitochondrial dysfunction, and cell apoptosis contribute to diabetes-induced myocardial injury [4–6]. Targeting these signaling pathways may represent a crucial strategy for combating the myocardial damage in diabetic population. Nitroxyl (HNO) is reported to target distinct signaling pathways to exert cytoprotective actions [7]. In vascular tissues, HNO donors induce vasodilatation, and attenuate vascular smooth muscle cell proliferation [7,8]. HNO donors suppress angiotensin II (Ang II) or endothelin-1 (ET1)-induced cardiomyocyte superoxide generation in primary cardiomyocytes [9]. HNO donors also exhibit antihypertrophic actions in the intact heart induced by pressure overload [10]. Chronic administration of HNO donor CXL-1020 attenuates the elevated left ventricle filling pressures, improves the end diastolic pressure volume relationship in rat models of diastolic heart failure [11]. Despite of these observations, whether HNO can be used to treat diabetic cardiomyopathy is still unknown. In addition, the underlying mechanisms by which HNO

* Corresponding author. Department of Pharmacology, Yong Loo Lin School of Medicine, National University of Singapore, Singapore, 117600, Singapore.
E-mail address: phcbjs@nus.edu.sg (J.-S. Bian).

https://doi.org/10.1016/j.redox.2020.101493
Received 25 October 2019; Received in revised form 24 February 2020; Accepted 3 March 2020
Available online 05 March 2020

exerts beneficial actions in the myocardium remain obscure. Considering the potential functions of HNO in cardiovascular system, we herein, hypothesized that exogenous HNO donor may attenuate diabetic cardiomyopathy injury in diabetic mice.

2. Material and methods

2.1. Chemicals and reagents

Dulbecco's Modified Eagle's Medium (DMEM), fetal bovine serum (FBS), and trypsin-EDTA were purchased from Hyclone Laboratories (South Logan, UT, USA). The RIPA lysis buffer was obtained from ThermoFisher Scientific Inc (Waltham, MA. USA). Cell culture plates were purchased from Costar Corning Inc. (Corning, CA, USA). Angeli's salt (AS), Piloty's acid, and WSP-1 (a reactive disulfide-containing fluorescent probe for H_2S detection) were procured from Cayman chemical company (Ann Arbor, MI. USA). Dihydroethidium (DHE), sodium hydrosulfide (NaHS), sodium nitroprusside (SNP), L-NAME (NG-Nitro-L-arginine Methyl Ester) and L-cysteine (L-cys) were obtained from Sigma-Aldrich (St. Louis, MO, USA). Click-iT™ Plus EdU (5-ethynyl-2′-deoxyuridine) Alexa Fluor™ 488 Imaging Kits, MitoSOX™, 4-amino-5-methylamino-2′,7′-difluorofluorescein diacetate (DAF-FM diacetate), Click-iT™ Plus TUNEL Assay for In Situ Apoptosis Detection, Alexa Fluor™ 488 dye were obtained from Invitrogen (Carlsbad, CA, USA). Nitric oxide (NO) assay kits, cell counting kit-8 (CCK-8) kits, and mitochondrial membrane potential assay kits with JC-1, as well as the kits for measurement of lactate dehydrogenase (LDH), malondialdehyde (MDA), superoxide dismutase (SOD) and glutathione (GSH) activities were purchased from Beyotime Institute of Biotechnology (Shanghai, China). Cell-Light™ EdUTP Apollo®567 TUNEL Cell Detection Kit was purchased from RiboBio (Guangzhou, China). Antibodies against CTH Antibody (F-1), $p22^{phox}$, $p47^{phox}$, Bax, Bcl-2, GAPDH, β-tublin, phosphorylated-eNOS, total-eNOS, caveolin-3 (Cav-3), and the horseradish peroxidase conjugated secondary antibodies were purchased from Santa Cruz BiotechnologyInc (Santa Cruz, CA. USA). Antibodies against cleaved-caspase-3 and α-actinin were obtained from Abcam (Cambridge, MA. USA).

2.2. Animals

All animal procedures were performed in accordance with the guidance of Institutional Animals Care and Use Committee at National of University of Singapore, and our animal project was approved (R18-0422). All experiments were adhered to the Care and Use of Laboratory Animal published by the US National Institutes of Health (NIH publication, 8th edition, 2011). The mice were purchased from InVivos (Singapore) and housed in a temperature-controlled and humidity-controlled room.

2.3. Induction of diabetes in mice

Diabetes mellitus was induced in male C57BL/6 mice aging from 8 to 10 weeks old by a single intraperitoneal (i.p.) injection of STZ (100 mg/kg), which was dissolved in 100 mM citrate buffer (pH 4.5) as depicted previously [12,13]. Control mice received an equivalent volume of citrate buffer. After one week, the mouse tail vein blood glucose levels were measured by the Roche Accu-Chek Active blood glucose monitor. The mice with a fasting blood glucose level more than 12 mmol/L were considered diabetic. All mice were allowed free access to standard laboratory chow and tap water for another 3 months. Eight weeks after STZ injection, the diabetic and control mice were randomly divided into two groups, which were received injection (i.p.) of normal saline or AS (10 mg/kg/day) for consecutive 4 weeks. In brief, four groups were included (1) vehicle-treated nondiabetic mice, (2) AS-treated nondiabetic mice, (3) vehicle-treated diabetic mice, and (4) AS-treated diabetic mice. At the end of the experiments, the mice were killed under anesthesia after cardiac function measurement. The body weight was recorded, and the blood samples, heart tissues were collected.

2.4. Echocardiography

The cardiac function was measured with a high-resolution echocardiography system (Vevo 2100, VisualSonics) as we previously described [14]. In short, the mice were anesthetized with isoflurane inhalation (1%) and maintained at 37 °C on a heating pad. All measurements were the average of six consecutive cardiac cycles and performed by the same operator. The following parameters were measured and calculated: left ventricular fractional shortening (FS), left ventricular ejection fraction (EF), heart rate (HR), left ventricular internal dimension (LVID) in diastole and systole (LVID,d and LVID,s, respectively), left ventricular posterior wall (LVPW) thickness in diastole and systole (LVPW,d and LVPW,s, respectively), and the interventricular septum (IVS) dimension in diastole and systole (IVS,d and IVS,s, respectively).

2.5. Histological analysis

The collected heart tissues were fixed, dehydrated, and then embedded in paraffin. The myocardium sections (5 μm) were stained with hematoxylin and eosin (HE) for histopathology or Sirius-red to examine collagen deposition under light Olympus BX50 microscopy. FITC-conjugated wheat germ agglutinin (WGA, Invitrogen Corp) was used to determine the myocyte cross-sectional area, and 4',6-diamidino-2-phenylindole (DAPI)was used to identify the nuclei. A single myocyte was measured using an image quantitative digital analysis system (Image Pro-Plus version 6.0). A minimum of 100 myocytes per mouse was selected for analysis in each group. Collagen and non-collagen components were red-stained and orange-stained, respectively. The slides were examined microscopically and the fibrotic area was determined by the area of myocardial collagen/the area of the field using Image Pro-Plus version 6.0 image analysis software (Media Cybernetics, Bethesda, MD, USA) using the same parameters. The percentage of the tissue stained was determined (in 6 fields per sample). The apoptosis of myocytes was assessed by a commercial TUNEL assay kit. The relative positive cells were quantified using Image J software.

2.6. Detection of HNO and H_2S in H9c2 cells

A thiol-based fluorescent probe (NitroxylFlour, a free gift from Dr Jefferson Chan) is a sensitive and selective probe for HNO detection [15]. In brief, the cells were incubated with NitroxylFlour (5 μM) in a serum-free cell media for 15 min before the probe solution is removed and replaced with fresh media. Then, NaHS (100 μM), nitroprusside (SNP, 100 μM), combination of SNP (100 μM) and NaHS (100 μM) or AS (100 μM) were added, respectively. After incubation of 15 min, the fluorescence signals were obtained by a fluorescence microscope (DMi 8; Leica, Microsystems, Germany), and the photomicrographs were quantified. A commercial specific fluorescent probe (WSP-1, 20 μM) was used to detect the endogenous H_2S in H9c2 cells as previously described [16,17]. The measured fluorescence intensity was normalized to the control cells.

2.7. Cell culture

The H9c2 embryonic rat heart-derived cell line (American Type Culture Collection, Rockville, MD, USA) was cultured in DMEM supplemented 10% FBS equilibrated with humidified incubator containing 5% CO_2 at 37 °C. H9c2 cells were pretreated with HNO scavenger L-cysteine (L-cys, 3 mM) for 30 min before AS treatment for another 30 min, and then stimulated by high glucose (HG, 33 mM) for 48 h. In other groups, H9c2 cells were pretreated with L-NAME (300 μM) for

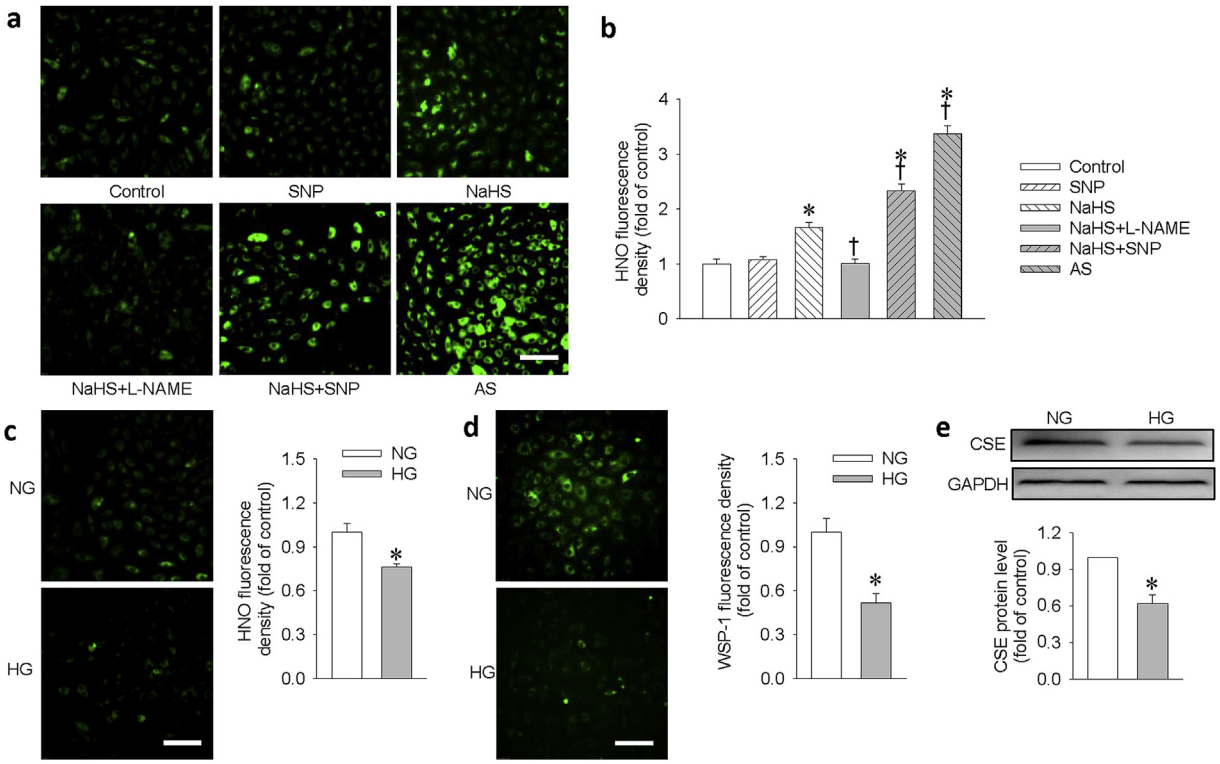

Fig. 1. Detection of HNO/H_2S in H9c2 cells. H9c2 cells were treated with PBS (control), NaHS (100 μM), SNP (100 μM), a combination of NaHS + SNP (100 μM each) or Angeli's Salt (100 μM) for 15 min. In NaHS + L-NAME group, the cells were pretreated with L-NAME (300 μM) for 30 min, and then incubated with NaHS (100 μM) for another 15 min. Under normal glucose (NG, 5.5 mM) and high glucose (HG, 33 mM) condition for 48 h, the basal HNO signals were captured with fluorescence microscope. (**a**) HNO signals in different groups. Scale bar = 100 μm. (**b**) The relative fluorescence signal intensity in response to NaHS, SNP, NaHS/SNP or AS. (**c**) HNO signals and relative fluorescence signal intensity under NG and HG conditions. Scale bar = 100 μm. (**d**) H9c2 cells were treated with NG or HG for 48 h. The H_2S level was examined by WSP-1 staining and quantifiably analyzed. (**e**) The protein expression of CSE was determined and quantifiably analyzed. Data were expressed as Mean ± SEM. *P < 0.05 vs. Control or normal glucose (NG). †P < 0.05 vs. NaHS. The results are from 4 to 6 independent experiments.

30 min before NaHS (100 μM) treatment for another 30 min and then stimulated by high glucose (HG, 33 mM) for 48 h. The primary neonatal mouse cardiomyocytes were isolated from 1 to 3 day-old C57BL/6 neonatal mice as previously depicted [18–20]. In brief, the hearts were digested by using 0.2 mg/ml collagenase type II (Worthington Biochemical, Lakewood, NJ) and 0.6 mg/ml pancreatin (Sigma, MAK030, St. Louis, MO). The supernatant-containing suspended cells were cultured in minimum essential medium with 10% FBS for 2 h to remove non-myocytes. Then, the culture medium was changed 48 h after seeding to minimum essential medium containing 10% FBS with 1% penicillin-streptomycin. In order to mimic the increased glucose level in diabetes, the H9c2 cells or primary neonatal mouse cardiomyocytes were cultured in 5.5 mM D-glucose (normal glucose) or 33 mM D-glucose (HG, Sigma, St. Louis, MO, USA) as previous reports [21,22].

2.8. Cell viability assay and LDH release assay

CCK-8 kits were employed to evaluate H9c2 cell viability in accordance with the manufacturer's protocols. Briefly, the cells were plated into 96 wells at a density of 1×10^4 cells, to adhere overnight, and then treated with different chemicals for 48 h under normal glucose (NG, 5.5 mM) or high glucose (HG, 33 mM) condition [22,23]. Finally, 10 μl of the WST-8 mixture solution was added into each well, and incubated for 2 h at 37 °C. The absorbance was measured spectrophotometrically at 450 nm with a Varioskan Flash microplate reader from Thermo Electron Corporation (Waltham, MA. USA). EdU incorporation assay was used to probe the proliferation of H9C2 cells following the manufacturer's protocols. In short, the stimulated cells were labeled with an optimized EdU concentration (10 μM) for 2 h, followed by cell fixation and permeabilization, and the nucleus was stained with Hoechst 33342. Eventually, the EdU-positive cells and Hoechst 33342-stained cells were photographed by a fluorescence microscope (DMi 8; Leica, Microsystems, Germany). LDH release assay was carried out by a commercial LDH-cytotoxicity assay kit according to the manufacturer's suggestions. After 30 min coupled enzymatic assay in cell supernatants, the absorbance was determined with Varioskan Flash microplate reader at 490 nm.

2.9. JC-1 staining and TUNEL staining

Mitochondrial membrane potential (Δψm) was determined by the fluorescent dye JC-1. In brief, the cells were incubated with JC-1 for 20 min at 37 °C. Then, the cells were washed again with PBS, and the images for JC monomers (Green fluorescence; 535 nm) and JC aggregates (Red fluorescence; 570 nm) were photographed by a fluorescence microscope (DMi 8; Leica, Microsystems, Germany). Cell-LightTM EdUTP TUNEL (RiboBio, Guangzhou, China) was used to determine the cell apoptosis. In short, the cells were seeded onto 96 wells at a density of 1×10^4 cells and the challenged cells were washed, fixed and permeated with 0.5% Triton X-100 in PBS. The cells were then incubated with TdT enzyme-EdUTP mixture for 1 h at 37 °C, Apollo® dye was added for 30 min in the dark, and cells were finally stained by DAPI. The TUNEL-positive cells were captured by a fluorescence microscope (DMi 8; Leica, Microsystems, Germany).

2.10. Measurement of intracellular and mitochondrial ROS

Intracellular ROS levels were examined by the fluorescent probe DHE as previously described [24]. H9c2 cells or heart tissues were loaded with DHE (10 μM) for 30 min under a light-protected humidified

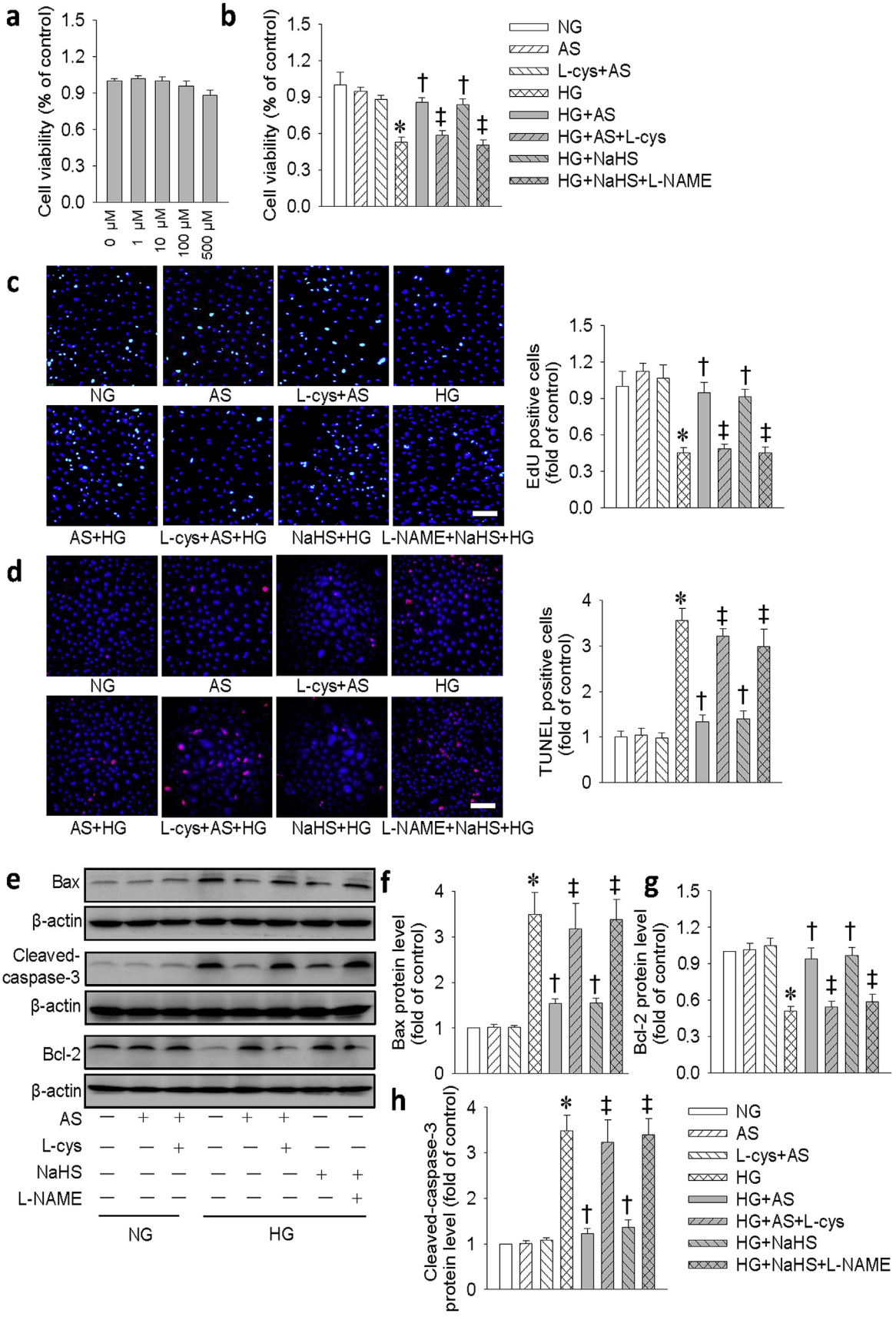

(caption on next page)

Fig. 2. HNO donor AS prevented HG-induced inhibition of cell viability and cell apoptosis in H9c2 cells. (**a**) H9c2 cells were treated with different doses of AS (0, 1, 10, 100, 500 μM) for 48 h, the cell viability was detected by CCK-8 assay. (**b**) H9c2 cells were pretreated with HNO scavenger L-cysteine (L-cys, 3 mM) for 30 min before AS treatment for another 30 min, and then stimulated by HG (33 mM) for 48 h. In other groups, H9c2 cells were pretreated with L-NAME (300 μM) for 30 min before NaHS (100 μM) treatment for another 30 min and then stimulated by HG (33 mM) for 48 h. The proliferation of H9c2 cells was assessed by CCK-8. (**c**) EdU incorporation assay. Green fluorescence (EdU) stands for cells with DNA synthesis, and blue fluorescence (DAPI) shows cell nuclei. Scale bar = 100 μm. (**d**) The cell apoptosis was determined with TUNEL assay, TUNEL positive nuclei in red fluorescent color and total nuclei staining with DAPI. Scale bar = 100 μm. (**e**) Represented blots showing the protein expressions of Bax, cleaved-caspase-3, and Bcl-2. (**f-h**) Bar group showing the relative quantification of Bax, Bcl-2 and cleaved-caspase-3. Data were expressed as Mean ± SEM. *P < 0.05 vs. NG (normal glucose), †P < 0.05 vs. HG (high glucose), ‡P < 0.05 vs. HG + AS or HG + NaHS. The data were calculated from 4 to 6 independent experiments. (For interpretation of the references to color in this figure legend, the reader is referred to the Web version of this article.)

chamber. After washing with PBS, the fluorescence signals were visualized using a fluorescence microscope (DMi 8; Leica, Microsystems, Germany). For measurement of mitochondrial ROS, H9c2 cells were treated with the mitochondrial superoxide-sensitive fluorescent dye MitoSOX Red (5 μM) for 30 min. Red fluorescence was indicated as mitochondrial superoxide, which was analyzed by a fluorescence microscope (DMi 8; Leica, Microsystems, Germany). The intracellular and mitochondrial ROS levels were quantified and normalized to the control cells.

2.11. Measurement of intracellular NO production

The stimulated cells were incubated with fluorescent indicator DAF-FM diacetate (2 μM) for 30 min for measuring intracellular NO production as previous report [25]. The green fluorescence was excited at 488 nm and imaged through a 525 nm long-path filter. In addition, Griess reagent was used to measure the nitrate content as previously described [26]. In other words, the NO levels were determined by a fluorometric method (Beyotime Biotechnology Inc., Shanghai, China) and standardized to the protein level.

2.12. Measurement of malondialdehyde (MDA) level, superoxide dismutase (SOD), and glutathione (GSH) activities

The content of MDA, SOD and GSH activities were determined using commercial assay kits following the manufacturer's instructions [27]. The samples were homogenized and then centrifuged at 12,000 × *g* for 15 min at 4 °C to obtain the supernatant. MDA content was detected by a Lipid Peroxidation MDA assay kit [28]. The activities of SOD and GSH were measured using a SOD reagent kit or a glutathione reductase assay kit, respectively. The final results were normalized to the protein content.

2.13. Transfection of siRNA

H9c2 cells were plated in 6-well plates to form a monolayer on the day before the transfection. After 30–50% confluence, H9c2 cells were transfected with a scrambled siRNA or Cav-3 siRNA (100 nM; Santa Cruz Biotechnology, Santa Cruz, CA) for 6 h by using Lipofectamine 2000 (Invitrogen, Carlsbad, CA, USA) according to the manufacturer's protocols [24]. The transfected cells were then washed twice with sterile PBS, changed with complete media and used for further experiments.

2.14. Immunofluorescence

The collected H9c2 cells were incubated with the primary anti-actinnin antibody overnight at 4 °C. After three washes with PBS, the cells were incubated with goat anti-mouse cross-adsorbed secondary antibody Alexa Fluor 488 (Invitrogen, Carlsbad, CA, USA). Nuclei were stained with DAPI. The fluorescence images were captured by a fluorescence microscope (DMi 8; Leica, Microsystems, Germany).

2.15. Immunoprecipitation

For co-immunoprecipitation assays, the collected cells were lysed in RIPA lysis buffer. The cell lysates were incubated with protein A/G agarose beads (Santa Cruz, CA. USA) and 2 μg of indicated antibodies or the same amount of control IgG overnight at 4 °C. In addition, the matrix was further washed 3 times with cold IP buffer and the immunoprecipitates were probed with primary antibodies in a Western blot analysis.

2.16. Quantitative or semi-quantitative PCR

Total RNA in each sample was extracted by using a Trizol reagent (Life Technologies, Gaithersburg, MD, USA) in accordance with the manufacturer's protocols. The equal RNA content (0.5 μg) was used to reverse transcriptase reactions using GoScript Reverse Transcription System (Promega Madison, WI, USA). In animal hearts, quantitative real-time PCR (qRT-PCR) was conducted by using GoTaq® Probe qPCR Master Mix (Promega Madison, WI, USA) under ABI Real-Time PCR System (Applied Biosystems ABI). Experimental Ct values were normalized to GAPDH by the $^{\Delta\Delta}$Ct method and relative mRNA expression was calculated from the value of threshold cycle (Ct). In cell samples, the cDNAs were synthesized from mRNAs and analyzed by semi-quantitative RT-PCR. All used primers were listed in Supplementary Table 1 and Table 2). The relative mRNA levels were normalized to GAPDH/β-actin expression.

2.17. Immunoblot analysis

Equal amounts of protein in each sample were loaded onto sodium dodecyl sulfate-polyacrylamide gel electrophoresis and transferred to PVDF membrane. The membranes were blocked with 5% skim milk in Tris-buffered saline containing 0.1% Tween 20 for 1 h at room temperature. Then, the membranes were incubated with the indicated primary antibodies overnight at 4 °C. After that, the membranes were incubated with horseradish peroxidase-conjugated secondary antibodies at room temperature for 1 h. The immune blots were developed using enhanced chemiluminescence system (Millipore, Billerica, MA, USA). The specific protein expression levels were normalized to the levels of house-keeping gene on the same PVDF membrane.

2.18. Statistical analysis

All results were presented as mean ± SEM. Comparison between two groups was analyzed using Student's t-test. Comparison among three or more groups was analyzed using ANOVA followed by Bonferroni test post hoc test (assuming equal variances). The criterion of statistical significance was $P < 0.05$.

3. Results

3.1. H_2S interacts with NO to generate HNO in H9c2 cells

With the aid of a modified thiol-based fluorescent probe, we examined the formation of HNO from the interaction of H_2S and NO in

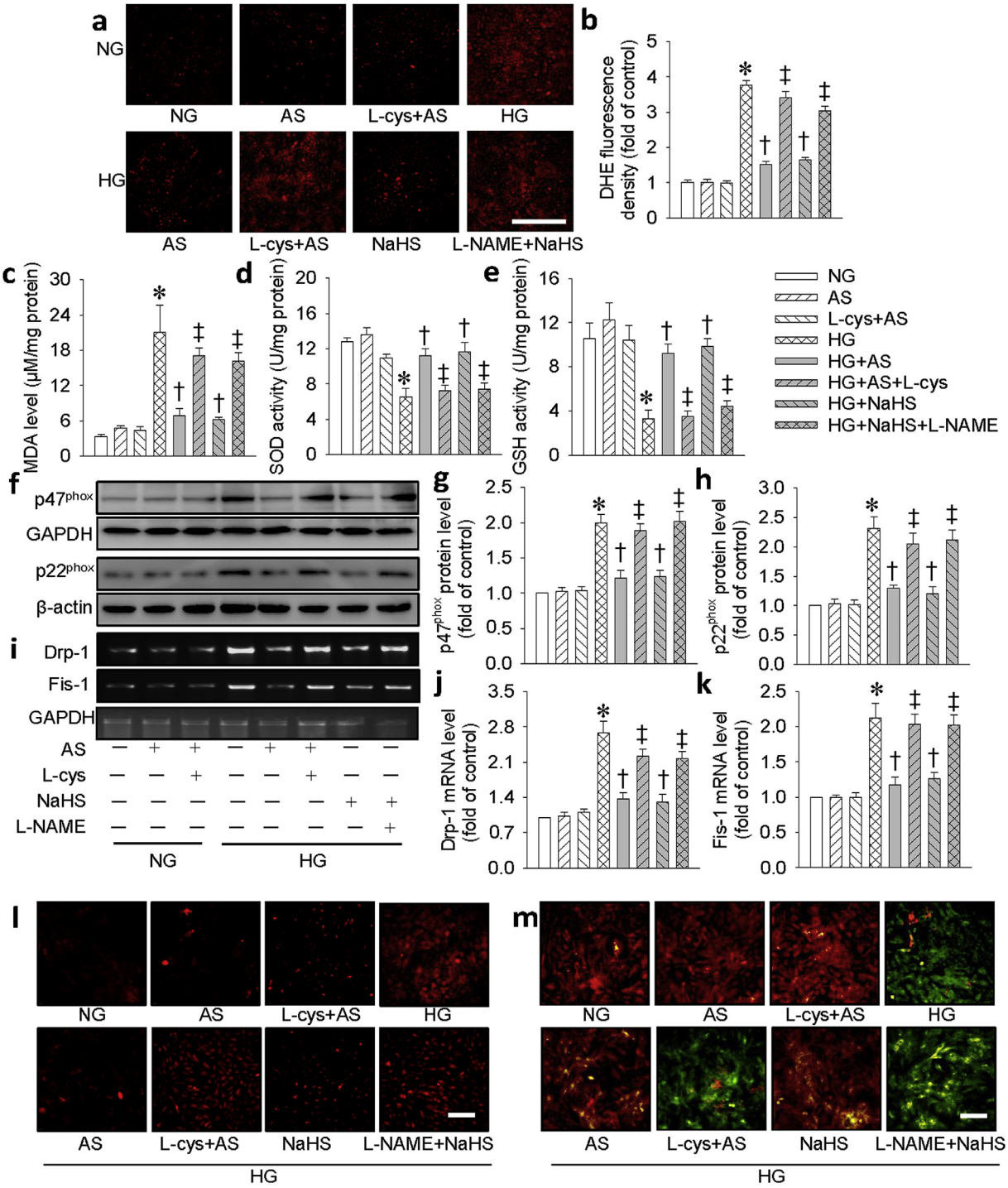

Fig. 3. HNO donor AS prevented HG-induced oxidative stress and mitochondrial disorder in H9c2 cells. (**a**) Images showing the levels of superoxide anions detected by DHE staining. Scale bar = 100 μm. (**b**) Relative fluorescence density of DHE staining. (**c**) Malondialdehyde (MDA) level. (**d**) Superoxide dismutase (SOD) activity. (**e**) Glutathione (GSH) activity. (**f**) Blots showing the protein expressions of $p47^{phox}$ and $p22^{phox}$. Bar graph showing the relative quantification of $p47^{phox}$ (**g**) and $p22^{phox}$ (**h**). (**i**) Images showing the level of Drp-1 and Fis-1. Bar graph showing the relative quantification of Drp-1 (**j**) and Fis-1 (**k**). (**l**) Representative photographs showing the mitochondrial ROS. Scale bar = 100 μm. (**m**) Mitochondrial membrane potential detected by JC-1 staining. Scale bar = 100 μm. Data were expressed as Mean ± SEM. *P < 0.05 vs. NG (normal glucose), †P < 0.05 vs. HG (high glucose), ‡P < 0.05 vs. HG + AS or HG + NaHS. The data were calculated from 4 to 6 independent experiments.

H9c2 cells. The basal HNO fluorescent signals were enhanced upon challenge with NaHS, a H_2S donor, but not by treatment with SNP, a NO donor. Pretreatment with L-NAME, an eNOS inhibitor, mitigated the production of HNO induced by NaHS. The amount of HNO produced by mixture of NaHS and SNP was comparable to that caused by AS, a HNO donor (Fig. 1a and b). Interestingly, treatment with HG obviously reduced the levels of the endogenous HNO (Fig. 1c) and H_2S (Fig. 1d). These findings suggest that H_2S may interact with endogenous NO to produce HNO in H9c2 cells. To study whether this is mediated by suppression of H_2S-generating enzyme activity, we determined the protein expression of cystathionine gamma-lyase (CSE), a key enzyme for H_2S production in H9c2 cells to generate H_2S. As shown in Fig. 1e,

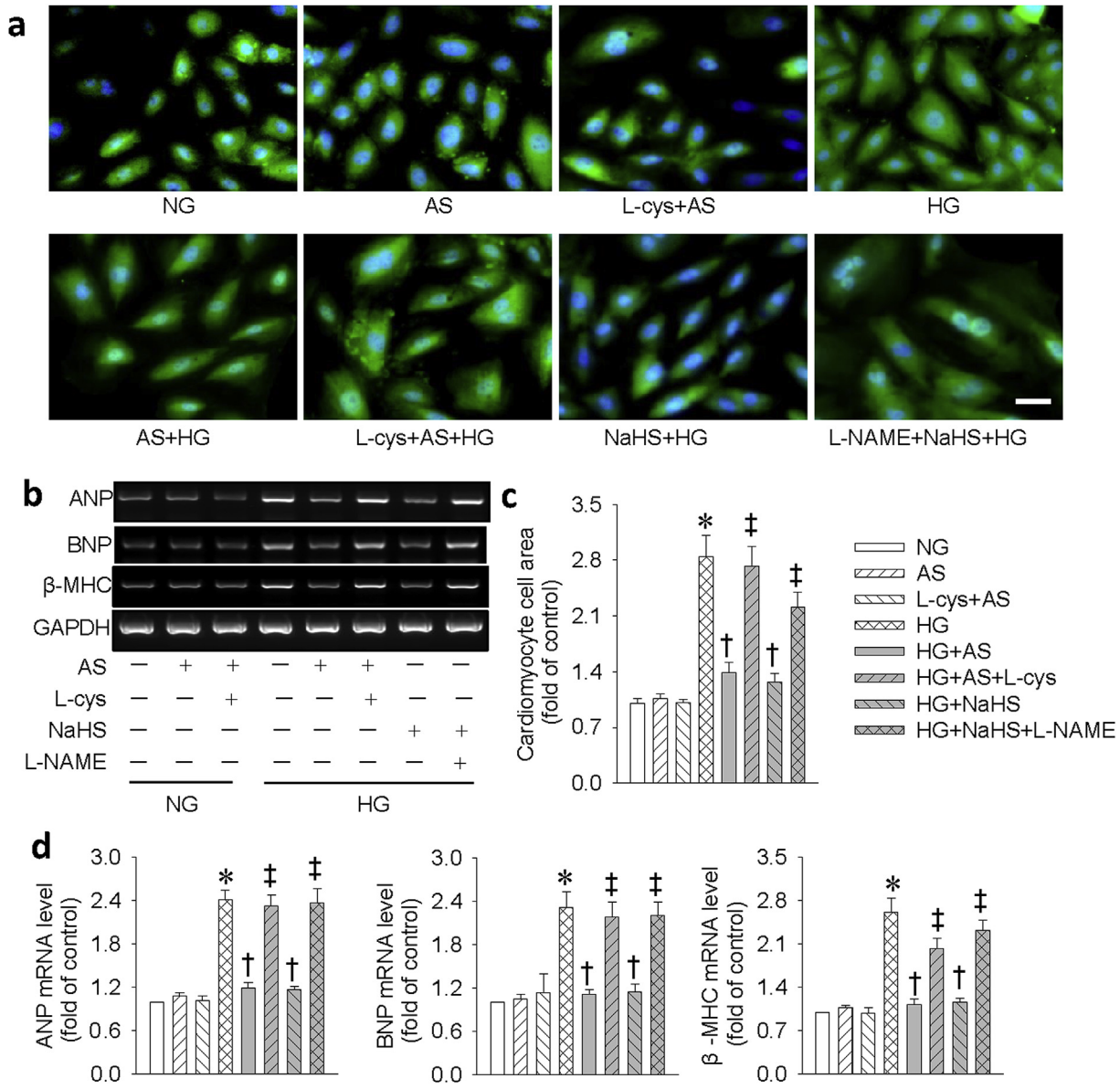

Fig. 4. HNO donor AS prevented HG-induced hypertrophy in H9c2 cells. (**a**) Representative immunofluorescence results showing the cell surface area by α-actinin staining. Scale bar = 50 μm. (**b**) Representative images showing the mRNA levels of ANP, BNP, β-MHC determined by reverse transcription–PCR. (**c**) Relative cardiomyocyte cell surface area. (**d**) The ANP, BNP, β-MHC mRNA levels were semiquantified by normalizing to GAPDH by densitometric analysis. Data were expressed as Mean ± SEM. *P < 0.05 vs. NG (normal glucose), †P < 0.05 vs. HG (high glucose), ‡P < 0.05 vs. HG + AS or HG + NaHS. The data were calculated from 4 to 6 independent experiments.

HG significantly reduced CSE expression in H9c2 cells, which was consistent with a previous report [29]. Taken together, our findings suggested that the decreased CSE-derived H_2S may be responsible for HG-induced suppression of HNO generation in H9c2 cells.

3.2. Effect of HNO on cell viability and apoptosis in H9c2 cells

To explore whether HNO produced any cytotoxic effect, we treated the H9c2 cells with different doses of HNO donor AS for 24 h. The results showed that HNO donor AS exhibited no significant effect on the viability of H9c2 cells (Fig. 2a). To determine the optimized dose of AS in protecting against HG-induced cell injury, a concentration response curve was carried out. Both CCK-8 assay and LDH release showed that AS dose-dependently restored the declined cell viability in HG-incubated H9c2 cells, reaching its maximal effects at the concentration of 100 μM (Fig. S1). As a result, the appropriate concentration of AS (100 μM) was chosen in the subsequent cell experiments. The decreased viability of H9c2 cells in HG group was restored by either AS or NaHS alone (Fig. 2b). The similar results were also found by measurement of LDH release (Fig. S2). EdU assay further demonstrated that HNO prevented HG-induced cell injury and promoted the viability of H9c2 cells (Fig. 2c). TUNEL assay showed that HG evoked cell apoptosis in H9c2 cells and this effect was significantly attenuated by AS and NaHS (Fig. 2d). To confirm the anti-apoptotic effect of AS, we measured the expressions of pro-apoptotic proteins (cleaved-caspase 3 and Bax) and anti-apoptotic protein Bcl-2 in H9c2 cells. As shown in Fig. 2e–h, both AS and NaHS attenuated the apoptotic effect of HG in H9c2 cells. Interestingly, the beneficial effect of HNO was abolished by an HNO scavenger L-cysteine (L-cys), whereas that of NaHS was attenuated by L-NAME, an eNOS inhibitor. These results imply that the beneficial effect of NaHS may be mediated by endogenous NO. We also examined the anti-apoptotic effect of HNO on primary neonatal mouse cardiomyocytes (Fig. S3). Similar results were found in these primary neonatal cardiomyocytes and further confirming that the beneficial effect of

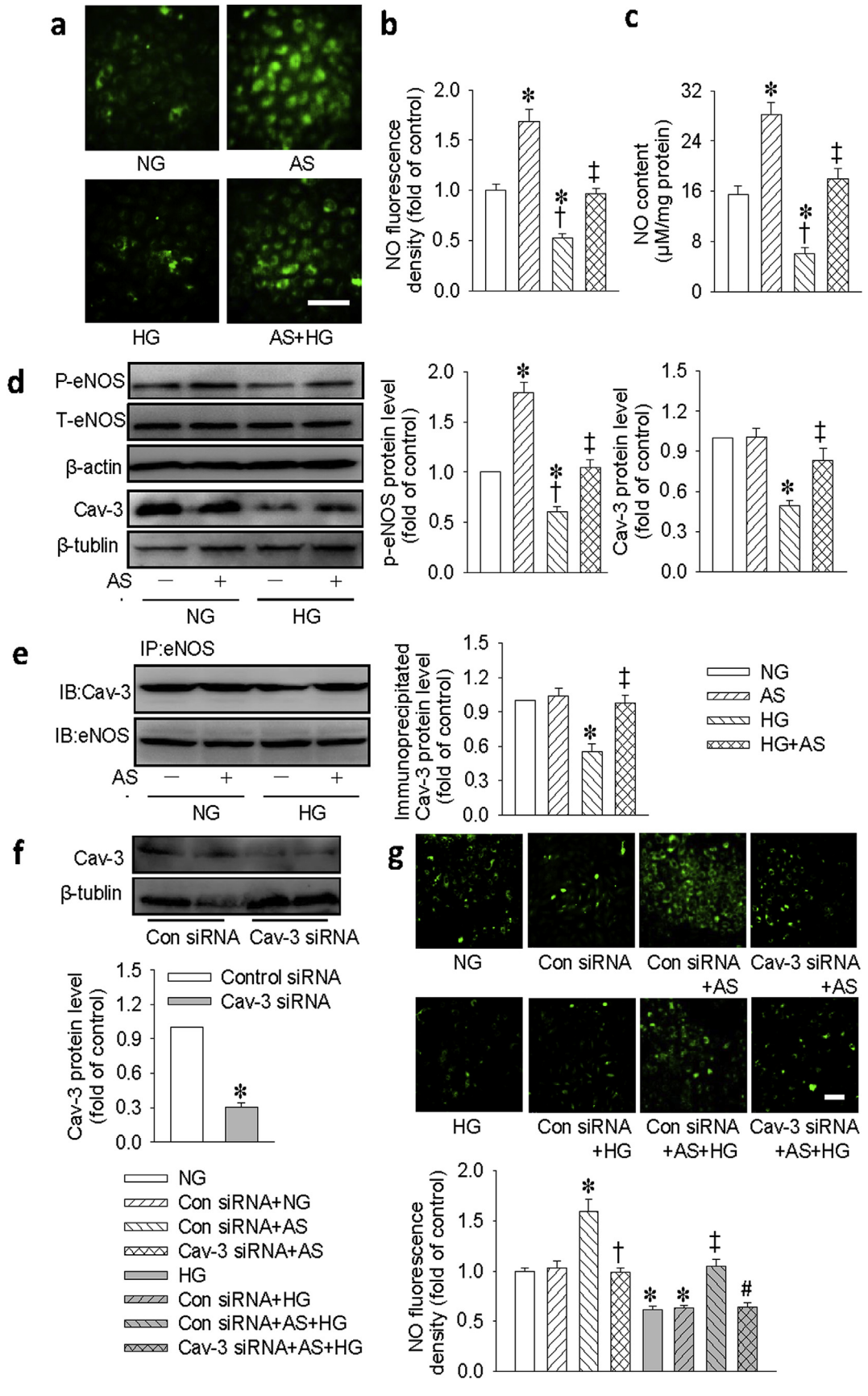

(caption on next page)

Fig. 5. HNO donor AS stimulated NO production via Cav-3/eNOS interaction in H9c2 cells. (**a**) Measurement of intracellular NO levels using DAF-FM diacetate. Scale bar = 100 μm. (**b**) Quantification of intracellular NO levels. (**c**) Measurement of intracellular NO levels using a fluorometric method. (**d**) Representative immunoblots and quantification of phosphorylated eNOS and Cav-3. (**e**) The lysates of cardiomyocytes containing equal amount of total protein were subjected to immunoprecipitation (IP) with e-NOS antibody and analyzed by immunoblot (IB) with Cav-3 antibody. (**f**) H9c2 cells were transfected with control or Cav-3 siRNA (100 nM) for 48 h. Representative immunoblot and quantification analysis of Cav-3. (**g**) H9c2 cells were transfected with control siRNA (100 nM) or Cav-3 siRNA (100 nM) for 6 h, before AS (100 μM) treatment for another 30 min, and then stimulated by HG (33 mM) for 48 h. Measurement of intracellular NO levels using DAF-FM diacetate. Scale bar = 100 μm. Data were expressed as Mean ± SEM. *P < 0.05 vs. NG (normal glucose) or Control (Con) siRNA. †P < 0.05 vs. AS or Control (Con) siRNA + AS, ‡P < 0.05 vs. HG (high glucose). #P < 0.05 vs. Control (Con) siRNA + AS + HG. The data were calculated from 4 to 6 independent experiments.

HNO in cardiac myocytes.

3.3. Effect of HNO on oxidative stress and mitochondrial dysfunction in H9c2 cells

Oxidative stress and mitochondrial dysfunction play central roles in the pathophysiology of HG-induced cell injury [30]. To determine whether the protective role of HNO against cell damage is related to reduction of ROS or mitochondrial functional homeostasis, redox status was detected by DHE probe, mitochondrial ROS were monitored by MitoSox Red and mitochondrial permeability transition was evaluated by JC-1 staining. As shown in Fig. 3a–c, AS and NaHS significantly reduced HG-induced ROS production (Fig. 3a and b) and MDA formation (Fig. 3c). Moreover, HG-reduced the activities of SOD (Fig. 3d) and GSH (Fig. 3e) were reversed by AS and NaHS, suggesting that both of them may preserve the activities of antioxidant enzymes. The contribution of NADPH oxidase in the generation of ROS was detected with western blotting assay. As shown in Fig. 3f–h, pretreatment with AS and NaHS abrogated the upregulated protein expressions of NADPH oxidase subunits $p47^{phox}$ (Fig. 3f, g) and $p22^{phox}$ (Fig. 3f, h) in H9c2 cells treated with HG. To study whether the effect of HNO was mediated by preserving mitochondrial function, we detected mitochondrial fission and membrane potential. As expected, AS and NaHS prevented HG–induced mRNA expressions of fission proteins Drp-1 (Fig. 3i and j) and Fis-1 (Fig. 3i, k). Similarly, AS reversed HG-induced mitochondrial ROS generation (Fig. 3l) and membrane potential loss in H9c2 cells (Fig. 3m). Notably, the above effects of AS were eliminated by L-cys, an HNO scavenger, confirming the effects of AS were mediated by HNO. Pretreatment with NaHS produced similar effects as AS. Interestingly, the protective effects of NaHS were significantly attenuated by L-NAME, indicating that the protective effects of NaHS may be attributed to the endogenous NO production. Consistent with the findings in cell line, HNO scavenger, L-cys, and eNOS inhibitor, L-NAME, abolished the effects of AS and NaHS, respectively, on NADPH oxidase subunits $p47^{phox}$ and $p22^{phox}$ protein levels in primary neonatal mouse cardiomyocytes (Fig. S4).

3.4. Effect of HNO on the cell size of H9c2 cells

We also investigated the effects of HNO on HG-induced cardiac hypertrophy. We detected cell morphology with immunofluorescence staining of α-actinin and mRNA levels of different hypertrophic markers. It was found that HG increased cell size (Fig. 4a,c) and the mRNA levels of hypertrophic markers (e.g. ANP, BNP and β-MHC (Fig. 4b,d). Pretreatment with AS or NaHS abolished these effects. Similarly, L-cys and L-NAME eliminated the protective action of HNO and NaHS, respectively. Likewise, this effect was also confirmed in primary neonatal mouse cardiomyocytes (Fig. S5).

3.5. Effect of SNP and Piloty's acid on H9c2 cell injury induced by HG

In biological medium, HNO donor AS may also yield NO [31,32]. We therefore observe whether HG-induced damages can be mitigated by NO. As shown in Fig. S6, NO donor SNP is insufficient to limit HG-induced cell vitality injury, apoptosis, ROS generation, and hypertrophy in H9c2 cells. In addition, the protective effects of HNO against HG-induced H9c2 cell injury were also validated by another HNO donor Piloty's acid [33,34], as pretreatment with Piloty's acid obviously relieved HG-induced cell toxicity, cell apoptosis, oxidative stress, and hypertrophy in H9c2 cells (Fig. S7). Taken together, it is highly probable that HNO donors, rather than NO donors, may be an attractive addition to the current therapeutic armamentarium for treating diabetic cardiomyopathy.

3.6. HNO stimulates NO production via Cav-3/eNOS interaction in cardiomyocytes

Of the three Cav isoforms in mammalian caveolae, Cav-3 is largely expressed in cardiomyocytes and it co-localizes to eNOS, thus permitting eNOS activation and NO release by cell surface receptor [35,36]. Therefore, Cav-3 is important for maintaining the function of NO, an endogenous inhibitor of hypertrophic signaling in the heart [37]. For this reason, we examined whether the protective effect of HNO against HG-induced cell injury was related to the recovery of Cav-3/eNOS association and its downstream NO signaling. Under basal conditions, the NO fluorescent intensity (Fig. 5a and b) and content (Fig. 5c) were enhanced by AS treatment. However, exposure to HG significantly inhibited NO production, and this effect was reversed by AS treatment (Fig. 5a–c). Accordingly, AS significantly attenuated the reduced p-eNOS and Cav-3 expressions in HG-incubated H9c2 cells (Fig. 5d). Co-IP analysis showed that eNOS remained constitutively associated with Cav-3 under NG conditions (Fig. 5e). However, HG stimulation reduced this association, whereas AS treatment restored this interaction. To examine the potential function of Cav-3 on NO production in H9c2 cells, we used siRNA to knockdown the Cav-3. As shown in Fig. 5f, transfection with Cav-3 siRNA significantly reduced the protein expression of Cav-3 and prevented the effect of AS on NO production under both normal and HG conditions (Fig. 5g). These results suggested that the Cav-3/eNOS/NO signaling pathway was a critical contributor to the protective effects of AS on HG-induced cell injury.

3.7. The effects of HNO are mediated by Cav-3/eNOS complex in cardiomyocytes

We next asked whether disruption of Cav-3/eNOS complex could eradicate the protective effects of AS, we treated H9c2 cells with inhibitor or siRNA to disrupt this complex. As expected, blockade of eNOS with L-NAME abolished the ability of AS to reverse the effects of HG on cell viability (Figs. S8a and c), cell apoptosis (Figs. S8b and d), oxidant stress (Figs. S8e and i), mitochondrial ROS production (Figs. S8f and j), and mitochondrial dysfunction (Fig. S8g), as well as cardiomyocyte hypertrophy (Figs. S8h and k) in H9c2 cells. The similar results were also found in H9c2 cells with deficiency of Cav-3 (Fig. S9). These results further reinforced our hypothesis that the Cav-3/eNOS complex was most likely required for AS to ameliorate HG-induced cell injury.

3.8. HNO attenuates diabetes-induced myocardial damage in vivo

Our *in vitro* results showed that HNO exerted a protective role against HG-induced cardiomyocyte injury. To further explore the pathophysiological significance of HNO in DCM, we used HNO donor AS to treat myocardial lesions in STZ-induced diabetic mice.

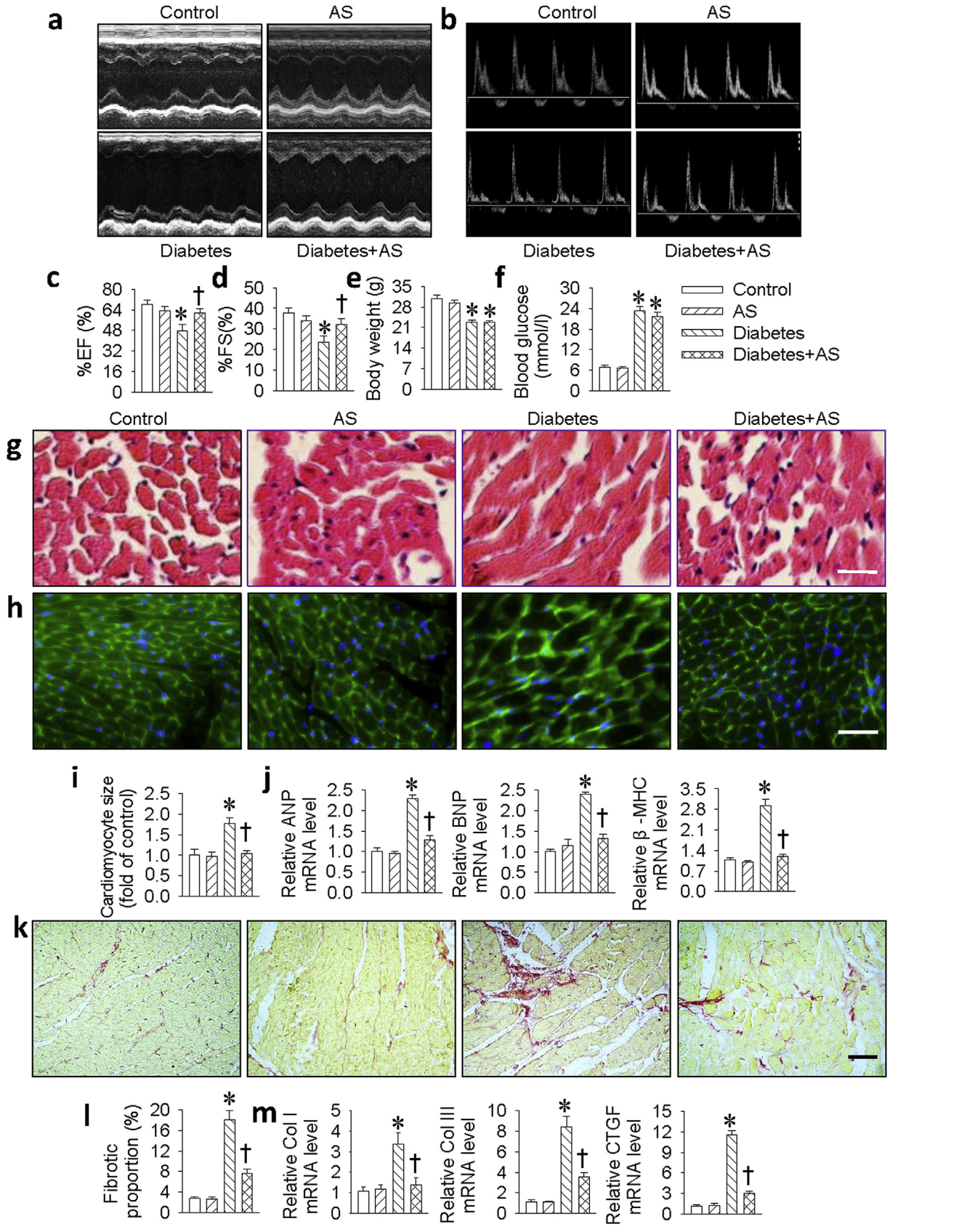

(caption on next page)

Fig. 6. HNO reversed cardiac dysfunction, cardiomyocyte hypertrophy, fibrosis in diabetic mice. (**a&b**) Cardiac diameter and function were measured by Echocardiography. (**c**) Analysis of left ventricular ejection fraction (EF). (**d**) Analysis of left ventricular fractional shortening (FS). (**e**) Body weight. (**f**) Fasting blood glucose. The cardiomyocyte size in mice heart was assessed by H&E staining (**g**) or Wheat germ agglutinin (WGA) staining (**h**), respectively. Scale bar = 50 μm. (**i**) Relative cross-sectional area of cardiomyocytes. (**j**) The mRNA levels of cardiomyocyte hypertrophy markers including ANP, BNP and β-MHC determining by real-time PCR. (**k**) The cardiac fibrosis was determined by Sirius red staining. Scale bar = 50 μm. (**l**) Percentage of cardiac fibrosis. (**m**) The mRNA levels of cardiomyocyte fibrotic markers including Collagen I (Col I), Collagen III (Col III) and CTGF determining by real-time PCR. Data were expressed as Mean ± SEM. *P < 0.05 vs. Control, †P < 0.05 vs. Diabetes. The data were calculated from 7 to 10 independent experiments. (For interpretation of the references to color in this figure legend, the reader is referred to the Web version of this article.)

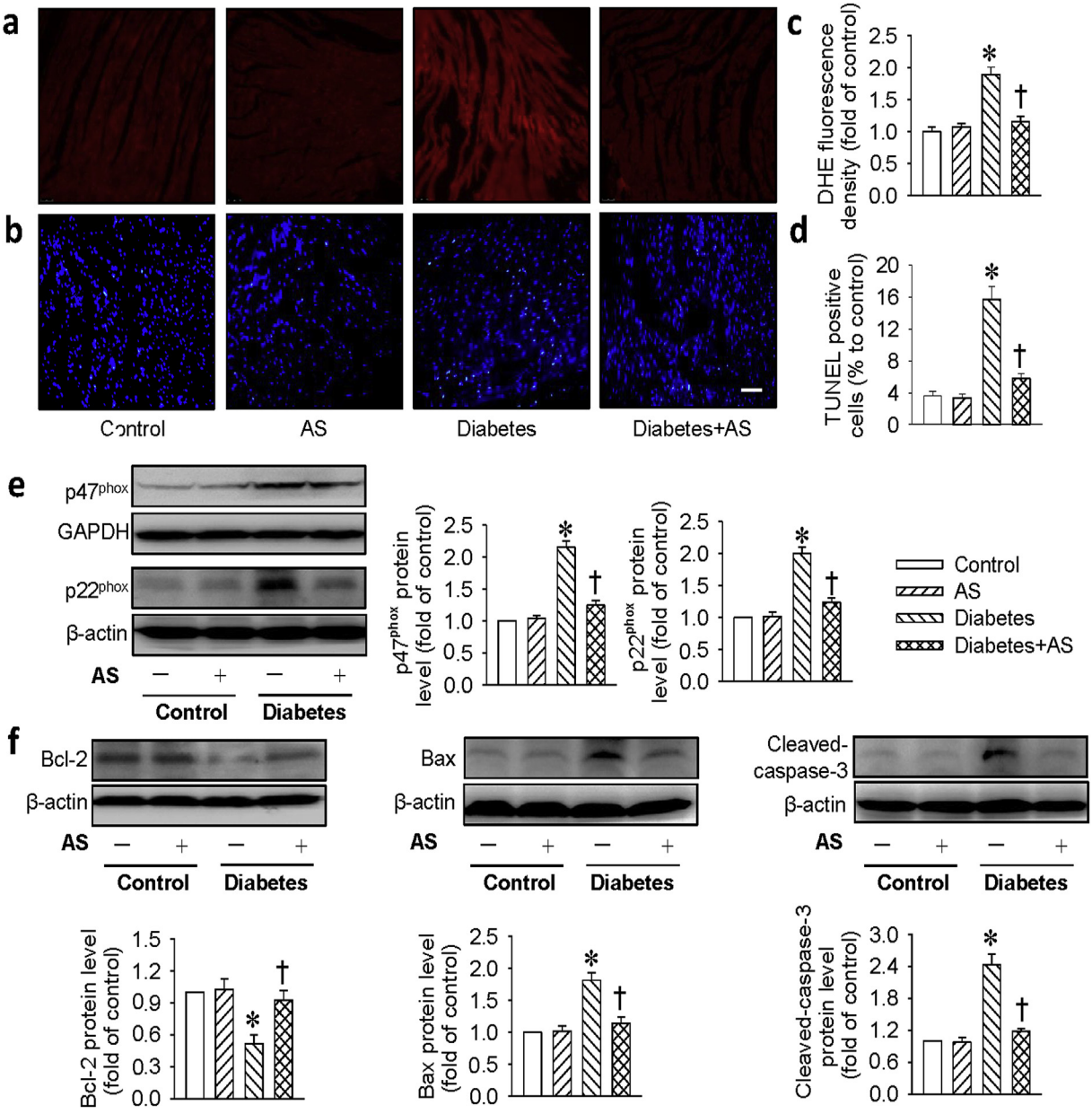

Fig. 7. HNO attenuated cardiomyocyte oxidative stress and apoptosis in diabetic mice. (**a&c**) The cardiomyocyte section was stained with DHE (10 μM), and the fluorescence intensity was calculated and normalized to the control. Scar bar = 50 μm. (**b&d**) The cardiomyocyte apoptosis was determined by TUNEL staining and analyzed, arrow indicated the apoptotic cardiomyocytes. Scar bar = 50 μm. (**e**) Represented blots and relative quantification of the protein expressions of $p47^{phox}$ and $p22^{phox}$. (**f**) Represented blots and relative quantification of the protein expressions of Bcl-2, Bax and cleaved-caspase-3. Data were expressed as Mean ± SEM. *P < 0.05 vs. Control, †P < 0.05 vs. Diabetes. The data were calculated from 6 to 10 independent experiments.

Echocardiography results demonstrated that the decreased ejection fraction (EF) and fractional shortening (FS) in diabetic mice were remarkably ameliorated by AS treatment, suggesting a protective role of HNO in cardiac function during the progression of DCM (Fig. 6a–d). Furthermore, as shown in Table S3, diabetic mice showed a decrease in cardiac structure parameters (IVS and LVPW; diastolic and systolic). These deficits were significantly reversed in AS-treated diabetic mice. All cardiac structural and functional parameters in AS-treated diabetic mice were similar to non-diabetic control mice. In comparison with control mice, STZ-induced diabetic mice exhibited relatively lower body weight (Fig. 6e) and increased blood glucose level (Fig. 6f) at the end of the experiment. However, we failed to see the protective effects

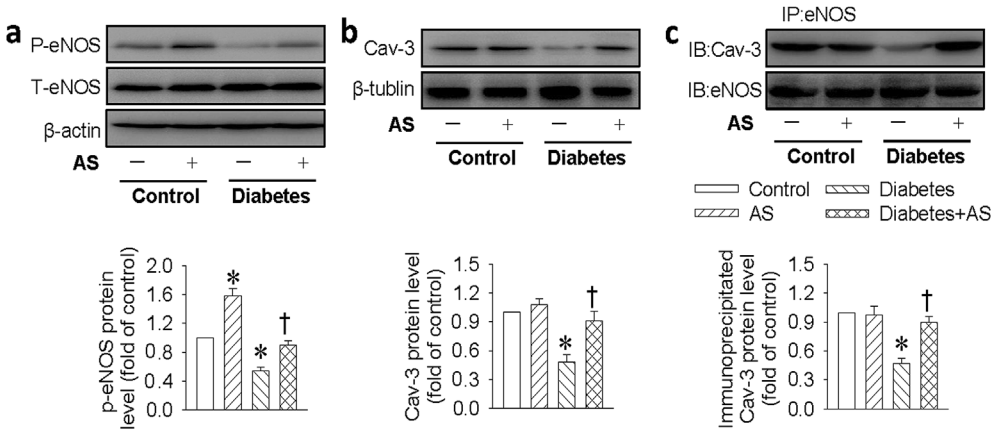

Fig. 8. HNO promoted eNOS/Cav-3 complex formation in diabetic hearts. (**a**) Represented blots and quantification analysis of phosphorylated eNOS. (**b**) Represented blots and quantification analysis of Cav-3 protein. (**c**) The eNOS/Cav-3 interaction in cardiac tissues was determined by immunoprecipitation. Data were expressed as Mean ± SEM. *P < 0.05 vs. Control, †P < 0.05 vs. Diabetes. The data were calculated from 4 to 6 independent experiments.

of AS on these two parameters. Furthermore, the myocardial structure was examined by H&E staining (Fig. 6g), WGA staining (Fig. 6h) and Sirius red staining (Fig. 6k). The diabetic hearts exhibited the structural abnormalities, such as the enlarged cardiomyocyte area (Fig. 6i) and cardiac fibrosis (Fig. 6l), but there was no significant evidence of these abnormalities in the heart tissues of diabetic mice treated with AS. Consistently, the mRNA expressions of hypertrophic markers (ANP, BNP, β-MHC, Fig. 6j) and fibrotic markers (Collagen I, Collagen III and CTGF, Fig. 6m) were highly increased in diabetic hearts. However, administration of AS prevented these increased hypertrophic and fibrotic parameters in diabetic mice.

Consistent with *in vitro* results, DHE staining in the heart tissues demonstrated that the levels of ROS were much lower in diabetic mice treated with AS (Fig. 7a, c). In addition, the oxidative stress protein markers, such as NADPH oxidase subunits $p47^{phox}$ and $p22^{phox}$protein levels were suppressed by AS in diabetic mice (Fig. 7e). We also assessed the effect of AS on the cell apoptosis in the heart tissues of diabetic mice. As shown in Fig. 7b, d, the increased TUNEL-positive cells in diabetic hearts were remarkably counteracted by AS treatment. Furthermore, the downregulated protein levels of Bcl-2 in diabetic mice were almost turned back to normal level after administration of AS (Fig. 7f). The protein levels of cleaved-caspase 3 and Bax were decreased to similar levels as control mice when diabetic mice were treated with AS (Fig. 7f). These results clearly indicated that AS prevented myocardial damage induced by diabetes.

3.9. HNO attenuates diabetes-interrupted Cav-3/eNOS complex in vivo

To test whether the Cav-3/eNOS complex was impaired under HG condition *in vivo*, the Cav-3/eNOS complex and downstream NO signaling was also examined in diabetic hearts. Similar to *in vitro* results, the downregulated phosphorylated eNOS and Cav-3 levels, as well as the impaired Cav-3/eNOS interaction were observed in the heart tissues from diabetic mice, but these abnormalities were remarkably reversed by HNO donor AS treatment (Fig. 8).

4. Discussion

DCM is featured by complex changes including cardiomyocyte hypertrophy, fibrosis and ventricular dysfunction [12]. However, the precise mechanisms of DCM have not been fully elucidated. Therefore, identification of novel modulators or new ideal drugs in DCM is highly warranted. In the present study, our data revealed that HG stimulation decreased cell viability, increased cell apoptosis and oxidative stress, accompanied by reduced HNO formation in cardiomyocytes, while these changes were reversed by HNO donor AS. In mice, STZ-induced hypertrophy, fibrosis, and cardiac dysfunction were retarded by administration of AS. Mechanistically, we demonstrated that AS promoted the complex formation of Cav-3/eNOS, thereby reducing hyperglycemia-induced cardiomyocyte damages *in vitro* and *in vivo* (Fig. S10).

Cardiovascular complications are the major cause of mortality and morbidity in diabetic subjects [3]. The pathophysiology mechanisms underlying diabetes-induced cardiac damages are complex and multifactorial, while cardiomyocyte apoptosis, oxidative stress and mitochondrial dysfunction are taken as key contributors [38]. A plethora of evidence has demonstrated that the decreased cell viability, enhanced cell apoptosis and ROS generation, increased cardiomyocyte hypertrophy, as well as the dissipation of mitochondrial membrane potential are observed in H9c2 cells exposed to HG stimulation [39–41]. The cardiovascular functions of HNO have been recently investigated, it enhances heart contractility and induces vasodilation [7]. HNO donors are reported to suppress cardiomyocyte superoxide generation and hypertrophy [9,10]. H_2S is described as a gasotransmitter that protects against HG-induced cardiomyocyte injury and inflammation, including cell cytotoxicity, apoptosis and ROS overproduction [42]. We found that exogenous HNO and H_2S relieved HG-trigger cell cytotoxicity and apoptosis, excessive ROS production and impaired mitochondrial function in H9c2 cells, suggesting that both HNO and H_2S could protect cardiac cells against HG-induced myocardial damage.

Notably, the chemical interaction between H_2S and NO to form HNO in many biological systems has gain substantial attention [43–47]. Specifically, blockade of NO production by L-NAME reversed the proliferative effect of H_2S on endothelial cells [48]. Incubation of cultured vascular smooth muscle cells with NO donor drugs significantly enhanced the transcriptional level of CSE and H_2S production [49]. Considering the functional and protective roles of HNO in cardiovascular system, the elucidation of HNO formation by H_2S–NO crosstalk would improve our understanding of the pathogenic mechanisms of HNO in cardiovascular ailments. In the current study, our data confirmed that both HNO donor AS and H_2S donor NaHS significantly elevated the HNO fluorescence intensity in H9c2 cells, which were prevented by HNO scavenger L-cys or nitric oxide synthase inhibitor L-NAME, respectively. Similarly, the mixture of both H_2S donor NaHS and NO donor SNP also produced the formation of HNO. These results proposed that the crosstalk between H_2S and NO may be responsible for the endogenous formation of HNO, which may be of physiological significance in the heart. Intriguingly, we found that the endogenous HNO was reduced in H9c2 cells upon HG challenge, the reduction of endogenous HNO formation in H9c2 cells may be attributed to the reduced H_2S-producing enzyme, CSE.

NO is indispensable for cardiovascular system homeostasis [50], and eNOS, an enzyme responsible for NO generation, may be of tremendous value for treatment of diabetic heart dysfunction [51,52]. Caveolins are highly expressed in cardiovascular cells, and they have been implicated in the regulation of endothelial barrier function, NO synthesis, cholesterol metabolism, and cardiac function [53]. Three

integral isoforms of caveolins are observed in mammalian caveolae (caveolin 1, 2, 3), among of which, Cav-3 is abundantly expressed in cardiac cells [35]. Cav-3 protein levels in the myocardium are depressed in diabetic conditions [52,54]. Cav-3 has also been shown to colocalize with eNOS [55], which may promote eNOS activation by both cell surface receptors and cellular surface NO release for intercellular signaling in cardiomyocytes [36]. Restoration of the Cav-3/eNOS/NO signaling pathway could ameliorate myocardial dysfunction and post-ischemic injury in diabetic rats [51]. The decreased Cav-3 protein level in diabetic hearts may result in caveolae dysfunction, which plays a vital role in eNOS/NO signaling impairment in cardiomyocytes. Our results showed that cardiomyocyte Cav-3 expression, eNOS phosphorylation, and NO production as well as colocalization of Cav-3 and eNOS were significantly reduced after HG exposure, and HNO treatment reversed these abnormal changes in HG-incubated cells. Additionally, disruption of Cav-3 by siRNA prevented the NO production induced by HNO. Importantly, blockade of Cav-3 or eNOS abolished the therapeutic effect of AS on H9c2 cells under HG condition. Furthermore, treatment of diabetic mice with AS enhanced the association of Cav-3 and eNOS, and increased Cav-3 and eNOS phosphorylation to comparable to those in the control mice. These data collectively suggest that the association of Cav-3 and eNOS is required for eNOS activation and subsequent NO generation in cardiomyocytes response to AS, thereby playing a protective role in diabetic hearts.

In addition to HNO, AS may also release NO in the biological conditions. However, AS-mediated protection is less likely caused by NO based on the following reasons. Firstly, decreased NO responsiveness, namely NO resistance, was found in many cardiovascular diseases, prominently in diabetes [56], even if pure NO is provided [57–59]. This suggests that NO-related signaling cascade is impaired in the disease situation. On the contrary, HNO-dependent signaling is still preserved in those disease conditions [60,61]. Interestingly, HNO donors can effectively attenuate NO resistance in the diabetic myocardium [62]. Secondly, our present results showed that HG-induced cell injury can be attenuated by two HNO donors, AS and Piloty's acid, but not by a NO donor, SNP. More importantly, a selective scavenger of HNO (L-cys) abolished the protective effects of AS against hyperglycemia-induced cell injury in H9c2 cells. Collectively, these results clearly suggest that the effects of AS is secondary to HNO rather than NO.

The characteristics of DCM are manifested by left ventricular diastolic and systolic dysfunction, accompanied by adverse structural changes including cardiomyocyte hypertrophy, apoptosis, oxidative stress, cardiac fibrosis and inflammation [63]. Doppler echocardiography results showed that diabetic mouse cardiac function was largely restored by HNO donor AS treatment. Additionally, HNO administration alleviated diabetes-induced cardiac remodeling such as cardiac hypertrophy, fibrosis, oxidative stress and apoptosis, as evidenced by both pathological staining and biochemical markers of myocardial injury. Thus, based on the above evidence, we concluded that the anti-apoptotic, anti-hypertrophic and anti-oxidant properties were involved in HNO-induced cardiac protection against diabetes. These beneficial actions seem to be a direct effect on the myocardium, which is not related with blood glucose regulation.

In summary, our present work vigorously demonstrated that the complex formation of Cav-3/eNOS is likely required for HNO to prevent hyperglycemia-induced cardiomyocyte damage at both cellular and animal levels, thus leading to improved diabetic cardiac function. Therefore, our results indicate that targeting the Cav-3/eNOS complex may be a promising therapeutic avenue in the treatment of DCM. It is noteworthy that the roles of HNO in cardiac damage induced by other diabetic models, such as the Akita mice (a model of insulin-deficient genetic diabetes), db/db mice, and ob/ob mice are undefined. Therefore, a comprehensive study is required to address this in the future. Moreover, further research will be needed to investigate the underlying mechanisms of HNO using cardiac specific Cav-3/eNOS overexpression or Cav-3/eNOS knockout mice.

5. Limitations

While there are many HNO donors currently available, the HNO-releasing agent most commonly used for animal studies is the prototypic HNO donor AS despite that its half-life is very short and it is also a co-generator of NO_2 [64–68]. For instance, *in vivo* administration of HNO donor AS is protective against vascular dysfunction [69,70], septic arthritis [71], neuropathic pain [72], and acute heart failure [73]. However, the present investigation has limitations inherent to any integrative *in vivo* studies because the exact fate of AS and its cellular interactions can not be defined. Similar to AS, H_2S is a signaling molecule that plays a variety of roles in mammalian systems although its short half-life (several minutes) and extensive reactivity [74–76]. Despite that NaHS can only provide instantaneous H_2S generation because of its short half-life, supplementation with the H_2S donor NaHS could attenuate the development of diabetic cardiomyopathy [77]. In similarity with H_2S, the biological effects of AS seem to be unaffected even if its biological half-life is very short. Anyway, it is indispensable to examine plasma AS concentration in the future research, and measurement of the pharmacokinetics of AS in animals is vital for a better understanding of its biological activities. Ultimately, the pure and longer-lasting HNO donors may be an attractive alternative for advancing the novel pharmacological actions of HNO.

Declaration of competing interest

The authors have no conflicts to declare.

Acknowledgements

This work was supported by research grants from Ministry of Education of Singapore Tier 2 Research grant (MOE2017-T2-2-029), and China Jiangsu Nature Science Foundation (BK20181185).

Appendix A. Supplementary data

Supplementary data to this article can be found online at https://doi.org/10.1016/j.redox.2020.101493.

References

[1] D.V. Nguyen, L.C. Shaw, M.B. Grant, Inflammation in the pathogenesis of microvascular complications in diabetes, Front. Endocrinol. 3 (2012) 170.
[2] V. Chavali, S.C. Tyagi, P.K. Mishra, Predictors and prevention of diabetic cardiomyopathy, Diabetes Metab. Syndr. Obes. 6 (2013) 151–160.
[3] K. Huynh, B.C. Bernardo, J.R. McMullen, R.H. Ritchie, Diabetic cardiomyopathy: mechanisms and new treatment strategies targeting antioxidant signaling pathways, Pharmacol. Ther. 142 (2014) 375–415.
[4] U. Varma, P. Koutsifeli, V.L. Benson, K.M. Mellor, L.M.D. Delbridge, Molecular mechanisms of cardiac pathology in diabetes - experimental insights, Biochim. Biophys. Acta 1864 (2018) 1949–1959.
[5] B.R. Goyal, A.A. Mehta, Diabetic cardiomyopathy: pathophysiological mechanisms and cardiac dysfuntion, Hum. Exp. Toxicol. 32 (2013) 571–590.
[6] G.K. Couto, L.R. Britto, J.G. Mill, L.V. Rossoni, Enhanced nitric oxide bioavailability in coronary arteries prevents the onset of heart failure in rats with myocardial infarction, J. Mol. Cell. Cardiol. 86 (2015) 110–120.
[7] M.L. Bullen, A.A. Miller, K.L. Andrews, J.C. Irvine, R.H. Ritchie, C.G. Sobey, B.K. Kemp-Harper, Nitroxyl (HNO) as a vasoprotective signaling molecule, Antioxidants Redox Signal. 14 (2011) 1675–1686.
[8] H. Kimura, Hydrogen sulfide and polysulfide signaling, Antioxidants Redox Signal. 27 (2017) 619–621.
[9] E.Q. Lin, J.C. Irvine, A.H. Cao, A.E. Alexander, J.E. Love, R. Patel, J.R. McMullen, D.M. Kaye, B.K. Kemp-Harper, R.H. Ritchie, Nitroxyl (HNO) stimulates soluble guanylyl cyclase to suppress cardiomyocyte hypertrophy and superoxide generation, PloS One 7 (2012) e34892.
[10] J.C. Irvine, N. Cao, S. Gossain, A.E. Alexander, J.E. Love, C. Qin, J.D. Horowitz, B.K. Kemp-Harper, R.H. Ritchie, HNO/cGMP-dependent antihypertrophic actions of isopropylamine-NONOate in neonatal rat cardiomyocytes: potential therapeutic advantages of HNO over NO, Am. J. Physiol. Heart Circ. Physiol. 305 (2013) H365–H377.
[11] N. Cao, Y.G. Wong, S. Rosli, H. Kiriazis, K. Huynh, C. Qin, X.J. Du, B.K. Kemp-Harper, R.H. Ritchie, Chronic administration of the nitroxyl donor 1-nitrosocyclo hexyl acetate limits left ventricular diastolic dysfunction in a mouse model of

diabetes mellitus in vivo, Circ. Heart Fail 8 (2015) 572–581.
[12] C. Zou, W. Li, Y. Pan, Z.A. Khan, J. Li, X. Wu, Y. Wang, L. Deng, G. Liang, Y. Zhao, 11beta-HSD1 inhibition ameliorates diabetes-induced cardiomyocyte hypertrophy and cardiac fibrosis through modulation of EGFR activity, Oncotarget 8 (2017) 96263–96275.
[13] P. Zhong, L. Wu, Y. Qian, Q. Fang, D. Liang, J. Wang, C. Zeng, Y. Wang, G. Liang, Blockage of ROS and NF-kappaB-mediated inflammation by a new chalcone L6H9 protects cardiomyocytes from hyperglycemia-induced injuries, Biochim. Biophys. Acta 1852 (2015) 1230–1241.
[14] F. Hua, Z. Wu, X. Yan, J. Zheng, H. Sun, X. Cao, J.S. Bian, DR region of Na(+)-K(+)-ATPase is a new target to protect heart against oxidative injury, Sci. Rep. 8 (2018) 13100.
[15] N.W. Pino, J. Davis 3rd, Z. Yu, J. Chan, NitroxylFluor: a thiol-based fluorescent probe for live-cell imaging of nitroxyl, J. Am. Chem. Soc. 139 (2017) 18476–18479.
[16] Y.J. Li, J. Chen, M. Xian, L.G. Zhou, F.X. Han, L.J. Gan, Z.Q. Shi, In site bioimaging of hydrogen sulfide uncovers its pivotal role in regulating nitric oxide-induced lateral root formation, PloS One 9 (2014) e90340.
[17] Y. Chen, H.Z. Mo, M.Y. Zheng, M. Xian, Z.Q. Qi, Y.Q. Li, L.B. Hu, J. Chen, L.F. Yang, Selenium inhibits root elongation by repressing the generation of endogenous hydrogen sulfide in Brassica rapa, PloS One 9 (2014) e110904.
[18] K. Iwatsubo, S. Minamisawa, T. Tsunematsu, M. Nakagome, Y. Toya, J.E. Tomlinson, S. Umemura, R.M. Scarborough, D.E. Levy, Y. Ishikawa, Direct inhibition of type 5 adenylyl cyclase prevents myocardial apoptosis without functional deterioration, J. Biol. Chem. 279 (2004) 40938–40945.
[19] J. Zhang, H. Xiao, J. Shen, N. Wang, Y. Zhang, Different roles of beta-arrestin and the PKA pathway in mitochondrial ROS production induced by acute beta-adrenergic receptor stimulation in neonatal mouse cardiomyocytes, Biochem. Biophys. Res. Commun. 489 (2017) 393–398.
[20] K.K. Durham, K.M. Chathely, K.C. Mak, A. Momen, C.T. Thomas, Y.Y. Zhao, M.E. MacDonald, J.M. Curtis, M. Husain, B.L. Trigatti, HDL protects against doxorubicin-induced cardiotoxicity in a scavenger receptor class B type 1-, PI3K-, and Akt-dependent manner, Am. J. Physiol. Heart Circ. Physiol. 314 (2018) H31–H44.
[21] M.P. Bhatt, Y.C. Lim, J. Hwang, S. Na, Y.M. Kim, K.S. Ha, C-peptide prevents hyperglycemia-induced endothelial apoptosis through inhibition of reactive oxygen species-mediated transglutaminase 2 activation, Diabetes 62 (2013) 243–253.
[22] M.X. Zhao, B. Zhou, L. Ling, X.Q. Xiong, F. Zhang, Q. Chen, Y.H. Li, Y.M. Kang, G.Q. Zhu, Salusin-beta contributes to oxidative stress and inflammation in diabetic cardiomyopathy, Cell Death Dis. 8 (2017) e2690.
[23] X. Zhou, W. Zhang, M. Jin, J. Chen, W. Xu, X. Kong, lncRNA MIAT functions as a competing endogenous RNA to upregulate DAPK2 by sponging miR-22-3p in diabetic cardiomyopathy, Cell Death Dis. 8 (2017) e2929.
[24] H.J. Sun, M.X. Zhao, X.S. Ren, T.Y. Liu, Q. Chen, Y.H. Li, Y.M. Kang, J.J. Wang, G.Q. Zhu, Salusin-beta promotes vascular smooth muscle cell migration and intimal hyperplasia after vascular injury via ROS/NFkappaB/MMP-9 pathway, Antioxidants Redox Signal. 24 (2016) 1045–1057.
[25] C.D. St Laurent, T.C. Moon, A.D. Befus, Measurement of nitric oxide in mast cells with the fluorescent indicator DAF-FM diacetate, Methods Mol. Biol. 1220 (2015) 339–345.
[26] D. He, M. Zhao, C. Wu, W. Zhang, C. Niu, B. Yu, J. Jin, L. Ji, B. Willard, A.V. Mathew, Y.E. Chen, S. Pennathur, H. Yin, Y. He, B. Pan, L. Zheng, Apolipoprotein A-1 mimetic peptide 4F promotes endothelial repairing and compromises reendothelialization impaired by oxidized HDL through SR-B1, Redox Biol. 15 (2018) 228–242.
[27] X. Zhu, Z. Zhou, Q. Zhang, W. Cai, Y. Zhou, H. Sun, L. Qiu, Vaccarin administration ameliorates hypertension and cardiovascular remodeling in renovascular hypertensive rats, J. Cell. Biochem. 119 (2018) 926–937.
[28] W. Chen, P. Zou, Z. Zhao, X. Chen, X. Fan, R. Vinothkumar, R. Cui, F. Wu, Q. Zhang, G. Liang, J. Ji, Synergistic antitumor activity of rapamycin and EF24 via increasing ROS for the treatment of gastric cancer, Redox Biol. 10 (2016) 78–89.
[29] C.Y. Tsai, S.Y. Wen, M.A. Shibu, Y.C. Yang, H. Peng, B. Wang, Y.M. Wei, H.Y. Chang, C.Y. Lee, C.Y. Huang, W.W. Kuo, Diallyl trisulfide protects against high glucose-induced cardiac apoptosis by stimulating the production of cystathionine gamma-lyase-derived hydrogen sulfide, Int. J. Cardiol. 195 (2015) 300–310.
[30] S. Roy, K. Trudeau, S. Roy, T. Tien, K.F. Barrette, Mitochondrial dysfunction and endoplasmic reticulum stress in diabetic retinopathy: mechanistic insights into high glucose-induced retinal cell death, Curr. Clin. Pharmacol. 8 (2013) 278–284.
[31] H. Nakagawa, Photocontrollable nitric oxide (NO) and nitroxyl (HNO) donors and their release mechanisms, Nitric Oxide 25 (2011) 195–200.
[32] H.J. Sun, W.T. Lee, B. Leng, Z.Y. Wu, Y. Yang, J.S. Bian, Nitroxyl as a potential theranostic in the cancer arena, Antioxidants Redox Signal. 32 (2020) 331–349.
[33] R. Smulik-Izydorczyk, M. Rostkowski, A. Gerbich, D. Jarmoc, J. Adamus, A. Leszczynska, R. Michalski, A. Marcinek, K. Kramkowski, A. Sikora, Decomposition of Piloty's acid derivatives - toward the understanding of factors controlling HNO release, Arch. Biochem. Biophys. 661 (2019) 132–144.
[34] K. Aizawa, H. Nakagawa, K. Matsuo, K. Kawai, N. Ieda, T. Suzuki, N. Miyata, Piloty's acid derivative with improved nitroxyl-releasing characteristics, Bioorg. Med. Chem. Lett 23 (2013) 2340–2343.
[35] M. Panneerselvam, H.H. Patel, D.M. Roth, Caveolins and heart diseases, Adv. Exp. Med. Biol. 729 (2012) 145–156.
[36] O. Feron, J.L. Balligand, Caveolins and the regulation of endothelial nitric oxide synthase in the heart, Cardiovasc. Res. 69 (2006) 788–797.
[37] T. Kempf, K.C. Wollert, Nitric oxide and the enigma of cardiac hypertrophy, Bioessays 26 (2004) 608–615.
[38] H. Bugger, E.D. Abel, Molecular mechanisms of diabetic cardiomyopathy, Diabetologia 57 (2014) 660–671.
[39] J. Chen, H. Mo, R. Guo, Q. You, R. Huang, K. Wu, Inhibition of the leptin-induced activation of the p38 MAPK pathway contributes to the protective effects of naringin against high glucose-induced injury in H9c2 cardiac cells, Int. J. Mol. Med. 33 (2014) 605–612.
[40] K.C. Cheng, W.T. Chang, Y. Li, Y.Z. Cheng, J.T. Cheng, GW0742 activates peroxisome proliferator-activated receptor delta to reduce free radicals and alleviate cardiac hypertrophy induced by hyperglycemia in cultured H9c2 cells, J. Cell. Biochem. 119 (2018) 9532–9542.
[41] S. You, J. Qian, C. Sun, H. Zhang, S. Ye, T. Chen, Z. Xu, J. Wang, W. Huang, G. Liang, An Aza resveratrol-chalcone derivative 6b protects mice against diabetic cardiomyopathy by alleviating inflammation and oxidative stress, J. Cell Mol. Med. 22 (2018) 1931–1943.
[42] P. Ye, Y. Gu, Y.R. Zhu, Y.L. Chao, Exogenous hydrogen sulfide attenuates the development of diabetic cardiomyopathy via the FoxO1 pathway, J. Cell. Physiol. 233 (2018) 9786–9798.
[43] Q.C. Yong, L.F. Hu, S. Wang, D. Huang, J.S. Bian, Hydrogen sulfide interacts with nitric oxide in the heart: possible involvement of nitroxyl, Cardiovasc. Res. 88 (2010) 482–491.
[44] M. Eberhardt, M. Dux, B. Namer, J. Miljkovic, N. Cordasic, C. Will, T.I. Kichko, J. de la Roche, M. Fischer, S.A. Suarez, D. Bikiel, K. Dorsch, A. Leffler, A. Babes, A. Lampert, J.K. Lennerz, J. Jacobi, M.A. Marti, F. Doctorovich, E.D. Hogestatt, P.M. Zygmunt, I. Ivanovic-Burmazovic, K. Messlinger, P. Reeh, M.R. Filipovic, H2S and NO cooperatively regulate vascular tone by activating a neuroendocrine HNO-TRPA1-CGRP signalling pathway, Nat. Commun. 5 (2014) 4381.
[45] Y. Zhou, Z. Wu, X. Cao, L. Ding, Z. Wen, J.S. Bian, HNO suppresses LPS-induced inflammation in BV-2 microglial cells via inhibition of NF-kappaB and p38 MAPK pathways, Pharmacol. Res. 111 (2016) 885–895.
[46] I.A. Szijarto, L. Marko, M.R. Filipovic, J.L. Miljkovic, C. Tabeling, D. Tsvetkov, N. Wang, L.A. Rabelo, M. Witzenrath, A. Diedrich, J. Tank, N. Akahoshi, S. Kamata, I. Ishii, M. Gollasch, Cystathionine gamma-lyase-produced hydrogen sulfide controls endothelial NO bioavailability and blood pressure, Hypertension 71 (2018) 1210–1217.
[47] Q.C. Yong, J.L. Cheong, F. Hua, L.W. Deng, Y.M. Khoo, H.S. Lee, A. Perry, M. Wood, M. Whiteman, J.S. Bian, Regulation of heart function by endogenous gaseous mediators-crosstalk between nitric oxide and hydrogen sulfide, Antioxidants Redox Signal. 14 (2011) 2081–2091.
[48] Z. Altaany, G. Yang, R. Wang, Crosstalk between hydrogen sulfide and nitric oxide in endothelial cells, J. Cell Mol. Med. 17 (2013) 879–888.
[49] W. Zhao, J. Zhang, Y. Lu, R. Wang, The vasorelaxant effect of H(2)S as a novel endogenous gaseous K(ATP) channel opener, EMBO J. 20 (2001) 6008–6016.
[50] L.J. Ignarro, C. Napoli, J. Loscalzo, Nitric oxide donors and cardiovascular agents modulating the bioactivity of nitric oxide: an overview, Circ. Res. 90 (2002) 21–28.
[51] W. Su, Y. Zhang, Q. Zhang, J. Xu, L. Zhan, Q. Zhu, Q. Lian, H. Liu, Z.Y. Xia, Z. Xia, N-acetylcysteine attenuates myocardial dysfunction and postischemic injury by restoring caveolin-3/eNOS signaling in diabetic rats, Cardiovasc. Diabetol. 15 (2016) 146.
[52] S. Lei, H. Li, J. Xu, Y. Liu, X. Gao, J. Wang, K.F. Ng, W.B. Lau, X.L. Ma, B. Rodrigues, M.G. Irwin, Z. Xia, Hyperglycemia-induced protein kinase C beta2 activation induces diastolic cardiac dysfunction in diabetic rats by impairing caveolin-3 expression and Akt/eNOS signaling, Diabetes 62 (2013) 2318–2328.
[53] J.P. Gratton, P. Bernatchez, W.C. Sessa, Caveolae and caveolins in the cardiovascular system, Circ. Res. 94 (2004) 1408–1417.
[54] S.V. Penumathsa, M. Thirunavukkarasu, S.M. Samuel, L. Zhan, G. Maulik, M. Bagchi, D. Bagchi, N. Maulik, Niacin bound chromium treatment induces myocardial Glut-4 translocation and caveolar interaction via Akt, AMPK and eNOS phosphorylation in streptozotocin induced diabetic rats after ischemia-reperfusion injury, Biochim. Biophys. Acta 1792 (2009) 39–48.
[55] L. Murfitt, G. Whiteley, M.M. Iqbal, A. Kitmitto, Targeting caveolin-3 for the treatment of diabetic cardiomyopathy, Pharmacol. Ther. 151 (2015) 50–71.
[56] S. Rajendran, Y.Y. Chirkov, Platelet hyperaggregability: impaired responsiveness to nitric oxide ("platelet NO resistance") as a therapeutic target, Cardiovasc. Drugs Ther. 22 (2008) 193–203.
[57] I. Seljeflot, B.B. Nilsson, A.S. Westheim, V. Bratseth, H. Arnesen, The L-arginine-asymmetric dimethylarginine ratio is strongly related to the severity of chronic heart failure. No effects of exercise training, J. Card. Fail. 17 (2011) 135–142.
[58] S.R. Willoughby, S. Rajendran, W.P. Chan, N. Procter, S. Leslie, E.A. Liberts, T. Heresztyn, Y.Y. Chirkov, J.D. Horowitz, Ramipril sensitizes platelets to nitric oxide: implications for therapy in high-risk patients, J. Am. Coll. Cardiol. 60 (2012) 887–894.
[59] V. Schachinger, M.B. Britten, A.M. Zeiher, Prognostic impact of coronary vasodilator dysfunction on adverse long-term outcome of coronary heart disease, Circulation 101 (2000) 1899–1906.
[60] N. Paolocci, T. Katori, H.C. Champion, M.E. St John, K.M. Miranda, J.M. Fukuto, D.A. Wink, D.A. Kass, Positive inotropic and lusitropic effects of HNO/NO- in failing hearts: independence from beta-adrenergic signaling, Proc. Natl. Acad. Sci. U. S. A. 100 (2003) 5537–5542.
[61] C.H. Leo, A. Joshi, J.L. Hart, O.L. Woodman, Endothelium-dependent nitroxyl-mediated relaxation is resistant to superoxide anion scavenging and preserved in diabetic rat aorta, Pharmacol. Res. 66 (2012) 383–391.
[62] C.X. Qin, J. Anthonisz, C.H. Leo, N. Kahlberg, A. Velagic, M. Li, E. Jap, O.L. Woodman, L.J. Parry, J.D. Horowitz, B.K. Kemp-Harper, R.H. Ritchie, Nitric oxide resistance, induced in the myocardium by diabetes, is circumvented by the nitric oxide redox sibling, nitroxyl, Antioxidants Redox Signal. 32 (2020) 60–77.
[63] Y.Q. Huang, X. Wang, W. Kong, [Diabetic cardiomyopathy], Sheng Li Ke Xue Jin Zhan 41 (2010) 31–36.
[64] K.M. Miranda, H.T. Nagasawa, J.P. Toscano, Donors of HNO, Curr. Top. Med. Chem. 5 (2005) 649–664.

[65] D.A. Guthrie, N.Y. Kim, M.A. Siegler, C.D. Moore, J.P. Toscano, Development of N-substituted hydroxylamines as efficient nitroxyl (HNO) donors, J. Am. Chem. Soc. 134 (2012) 1962–1965.
[66] K.M. Miranda, A.S. Dutton, L.A. Ridnour, C.A. Foreman, E. Ford, N. Paolocci, T. Katori, C.G. Tocchetti, D. Mancardi, D.D. Thomas, M.G. Espey, K.N. Houk, J.M. Fukuto, D.A. Wink, Mechanism of aerobic decomposition of Angeli's salt (sodium trioxodinitrate) at physiological pH, J. Am. Chem. Soc. 127 (2005) 722–731.
[67] A. Arcaro, G. Lembo, C.G. Tocchetti, Nitroxyl (HNO) for treatment of acute heart failure, Curr. Heart Fail. Rep. 11 (2014) 227–235.
[68] C.G. Tocchetti, B.A. Stanley, C.I. Murray, V. Sivakumaran, S. Donzelli, D. Mancardi, P. Pagliaro, W.D. Gao, J. van Eyk, D.A. Kass, D.A. Wink, N. Paolocci, Playing with cardiac "redox switches": the "HNO way" to modulate cardiac function, Antioxidants Redox Signal. 14 (2011) 1687–1698.
[69] B.M. Wynne, H. Labazi, Z.N. Carneiro, R.C. Tostes, R.C. Webb, Angeli's Salt, a nitroxyl anion donor, reverses endothelin-1 mediated vascular dysfunction in murine aorta, Eur. J. Pharmacol. 814 (2017) 294–301.
[70] J.C. Irvine, B.K. Kemp-Harper, R.E. Widdop, Chronic administration of the HNO donor Angeli's salt does not lead to tolerance, cross-tolerance, or endothelial dysfunction: comparison with GTN and DEA/NO, Antioxidants Redox Signal. 14 (2011) 1615–1624.
[71] L. Staurengo-Ferrari, K.W. Ruiz-Miyazawa, F.A. Pinho-Ribeiro, T.P. Domiciano, V. Fattori, S.S. Mizokami, J.S. Pelayo, J. Bordignon, F. Figueiredo, R. Casagrande, K.M. Miranda, W.A. Verri Jr., The nitroxyl donor Angeli's salt ameliorates Staphylococcus aureus-induced septic arthritis in mice, Free Radic. Biol. Med. 108 (2017) 487–499.
[72] D.T. Longhi-Balbinot, A.C. Rossaneis, F.A. Pinho-Ribeiro, M.M. Bertozzi, F.Q. Cunha, J.C. Alves-Filho, T.M. Cunha, J.P. Peron, K.M. Miranda, R. Casagrande, W.A. Verri Jr., The nitroxyl donor, Angeli's salt, reduces chronic constriction injury-induced neuropathic pain, Chem. Biol. Interact. 256 (2016) 1–8.
[73] K.Y. Chin, L. Michel, C.X. Qin, N. Cao, O.L. Woodman, R.H. Ritchie, The HNO donor Angeli's salt offers potential haemodynamic advantages over NO or dobutamine in ischaemia-reperfusion injury in the rat heart ex vivo, Pharmacol. Res. 104 (2016) 165–175.
[74] Y. Qian, J.B. Matson, Gasotransmitter delivery via self-assembling peptides: treating diseases with natural signaling gases, Adv. Drug Deliv. Rev. 110–111 (2017) 137–156.
[75] V. Vitvitsky, O. Kabil, R. Banerjee, High turnover rates for hydrogen sulfide allow for rapid regulation of its tissue concentrations, Antioxidants Redox Signal. 17 (2012) 22–31.
[76] D. Gero, R. Torregrossa, A. Perry, A. Waters, S. Le-Trionnaire, J.L. Whatmore, M. Wood, M. Whiteman, The novel mitochondria-targeted hydrogen sulfide (H2S) donors AP123 and AP39 protect against hyperglycemic injury in microvascular endothelial cells in vitro, Pharmacol. Res. 113 (2016) 186–198.
[77] X. Zhou, G. An, X. Lu, Hydrogen sulfide attenuates the development of diabetic cardiomyopathy, Clin. Sci. (Lond.) 128 (2015) 325–335.